

Supplementary Information

Quinoline-based TADF emitters exhibiting aggregation-induced emission for efficient non-doped organic light-emitting diodes

Yi-Fan Shen,^a Meng Li,^{*,b} Wen-Long Zhao,^a Yin-Feng Wang,^{a,b} Hai-Yan Lu^{*a} and Chuan-Feng Chen^{*a,b}

^a*University of Chinese Academy of Sciences, Beijing 100049, China.*

^b*Beijing National Laboratory for Molecular Sciences, CAS Key Laboratory of Molecular Recognition and Function, Institute of Chemistry, Chinese Academy of Sciences, Beijing 100190, China.*

E-mail: haiyanlu@ucas.ac.cn; limeng@iccas.ac.cn; cchen@iccas.ac.cn

Contents

1. General information.....	S2
2. Single crystal data and conformation.....	S3
3. Photophysical data.....	S5
4. NMR spectra.....	S9
5. High-resolution mass spectra.....	S12
6. DFT calculations.....	S13
7. HPLC analysis.....	S14
8. Device fabrication and characterization.....	S15
9. References.....	S21

1. General information

All the reagents and solvents were purchased from commercial sources and used without further purification. ^1H and ^{13}C NMR spectra were recorded on Brucker 300 MHz NMR spectrometers in CDCl_3 solutions. High resolution mass spectra were measured on a Thermo Fisher® Exactive high resolution LC-MS spectrometer. Thermal gravimetric analyses (TGA) were performed on a TA Instruments TGA 2050 thermal analyzer at a heating rate of 10 °C/min in nitrogen. Cyclic voltammetry was performed using a CHI600A analyzer with a scan rate of 100 mV/s at room temperature to investigate the oxidation potentials.

Single crystals of emitters suitable for X-ray diffraction analyses were obtained from their solution in CH_2Cl_2 . Crystal structures were solved with direct methods and refined with a full-matrix least-squares technique, using the SHELXS software package. UV-Vis spectra were recorded on PerkinElmer® Lambda 950 UV-Vis/NIR spectrometer, and the fluorescence spectra were recorded on HITACHI® F-7000 Fluorescence Spectrometer. The transient photoluminescence decay characteristics and temperature dependence experiments and absolute PL quantum yield were measured on an Edinburgh Instruments FLS980 spectrometer.

2. Single crystal data and conformation

Table S1 Single crystal data of compound **PTZ-QL**.

Empirical formula	$C_{21}H_{14}N_2S$	
CCDC No.	2016121	
Formula weight	326.40	
Temperature	169.97(13) K	
Crystal system	Monoclinic	
Space group	$P2_1/c$	
Unit cell dimensions	$a=7.97000(10)$ Å	$\alpha=90^\circ$
	$b=13.74990(10)$ Å	$\beta=99.3200(10)^\circ$
	$c=14.78660(10)$ Å	$\gamma=90^\circ$
Volume	$1599.02(3)$ Å ³	
Z	4	
Density(calculated)	1.356 g/cm ³	
Absorption coefficient	1.804 mm ⁻¹	
F(000)	680.0	
Crystal size	$0.25 \times 0.23 \times 0.21$ mm ³	
Theta range for data collection	8.836 to 151.098°	
index ranges	$-10 \leq h \leq 9, -17 \leq k \leq 13, -18 \leq l \leq 18$	
Reflections collected	11663	
Independent reflections	3154 [$R_{int}=0.0150$, $R_{sigma}=0.0113$]	
Data/restraints/parameters	3154/0/217	
Goodness-of-fit on F^2	1.045	
Final R indexes [$I \geq 2 \sigma(I)$]	$R_1 = 0.0309, wR_2 = 0.0816$	
R indexes (all data)	$R_1 = 0.0314, wR_2 = 0.0819$	
Largest diff. peak/hole	0.23/-0.30 e. Å ⁻³	

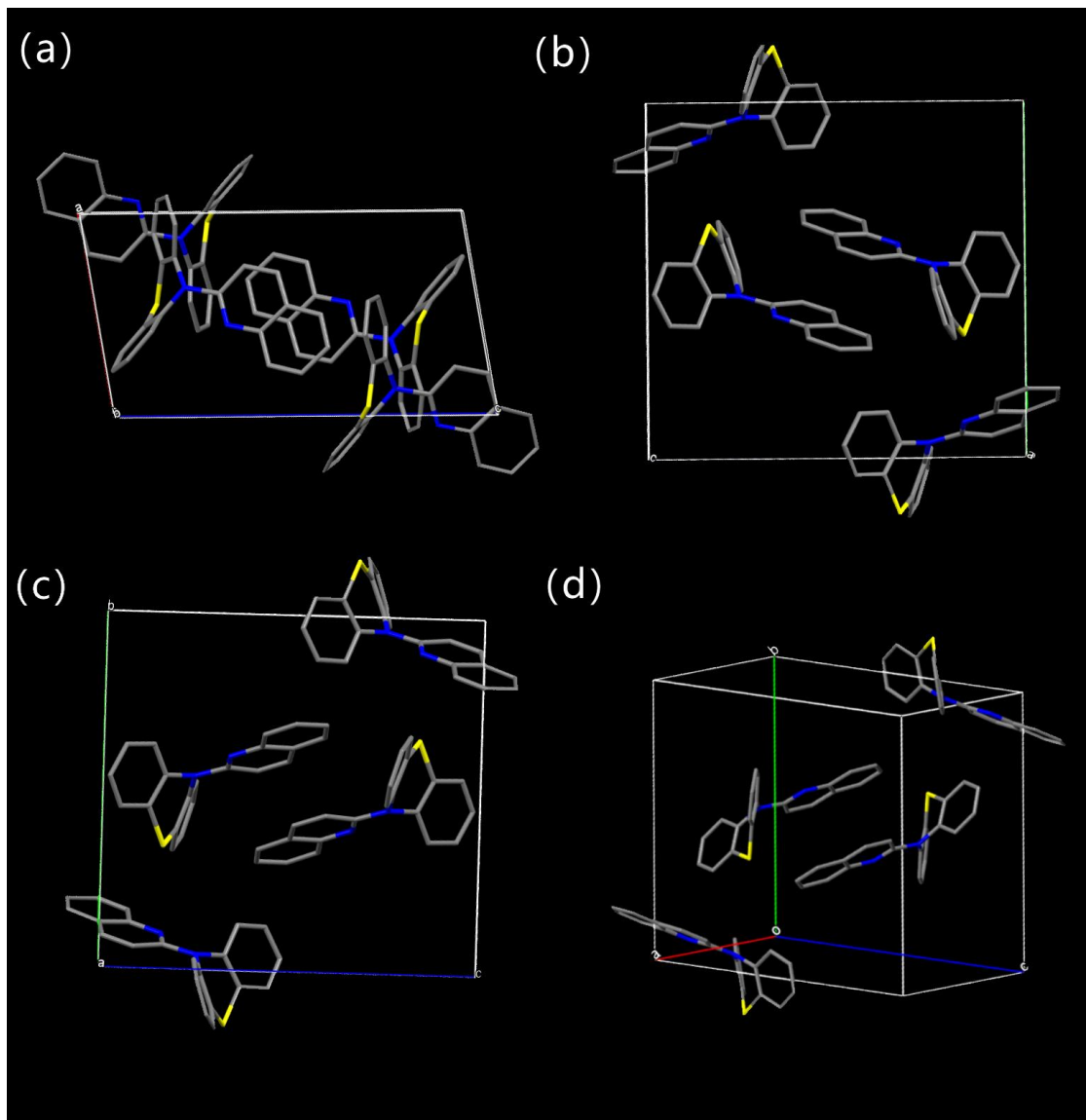


Fig. S1 Schematic molecular conformations and interactions in the crystal structure of **PTZ-QL**.

3. Photophysical data

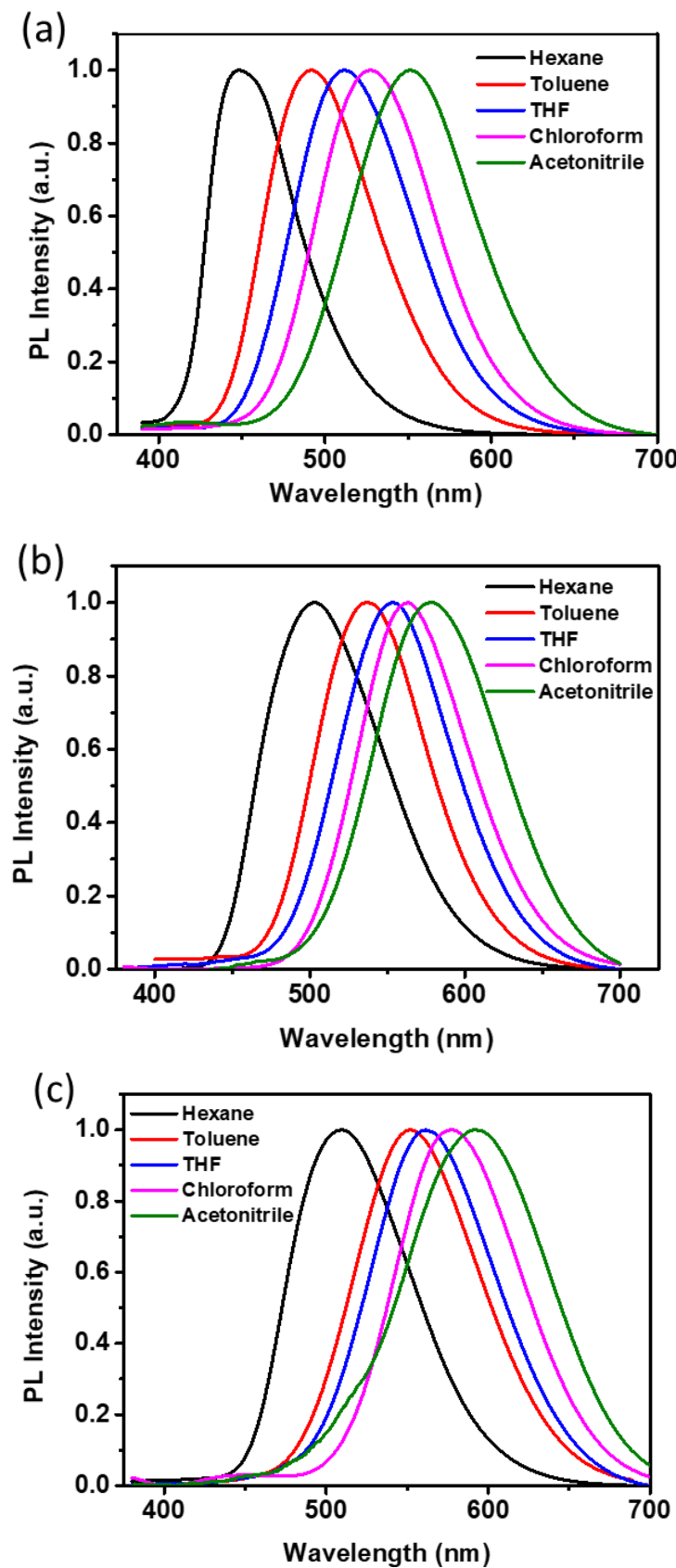


Fig. S2 Fluorescence spectra of (a) DMAC-QL, (b) PXZ-QL and (c) PTZ-QL in different solvents.

Table S2 Fluorescence emission peaks of **DMAC-QL**, **PXZ-QL** and **PTZ-QL** in different solvents.

Solvent	λ_{PL} (nm)		
	DMAC-QL	PXZ-QL	PTZ-QL
Hexane	448	503	510
Toluene	492	537	552
THF	511	554	561
Chloroform	528	564	577
Acetonitrile	552	579	592

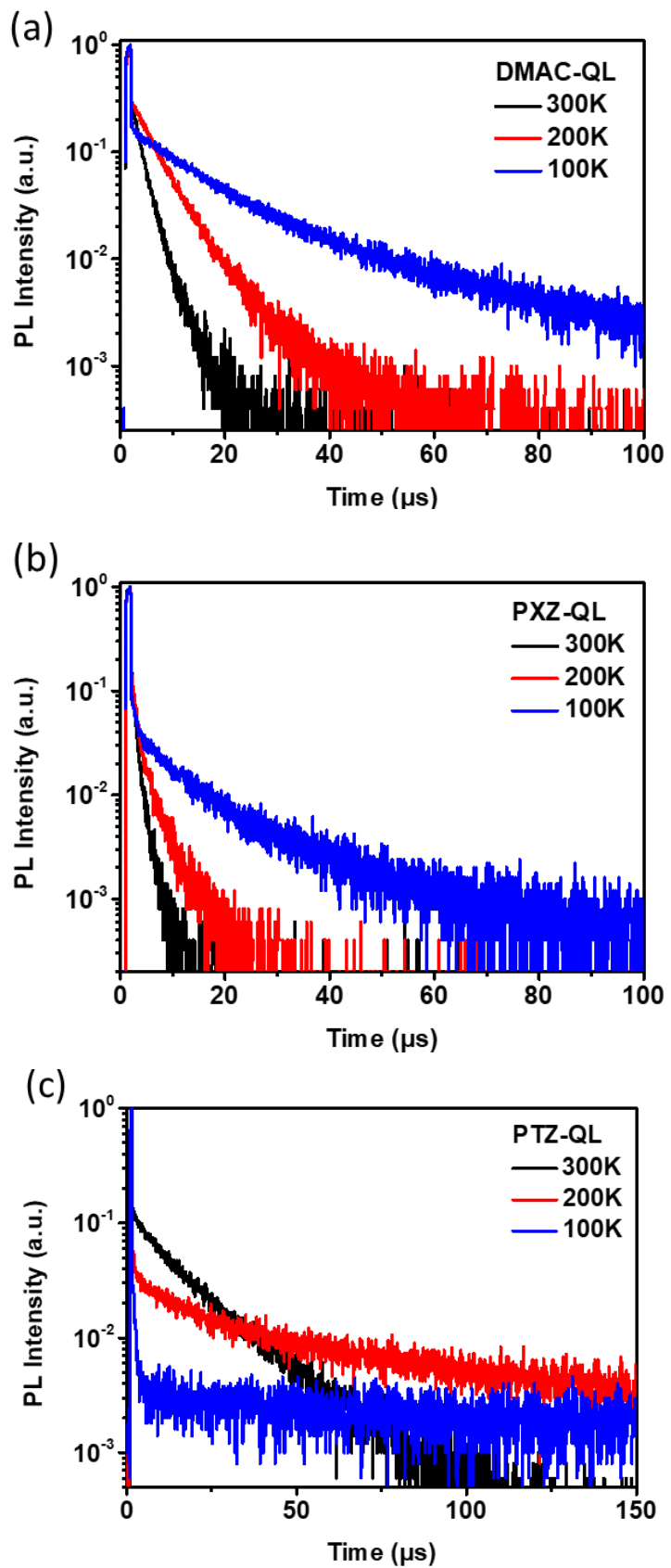


Fig. S3 Transient PL decay spectra of (a) DMAC-QL, (b) PXZ-QL and (c) PTZ-QL in neat films from 100 to 300 K.

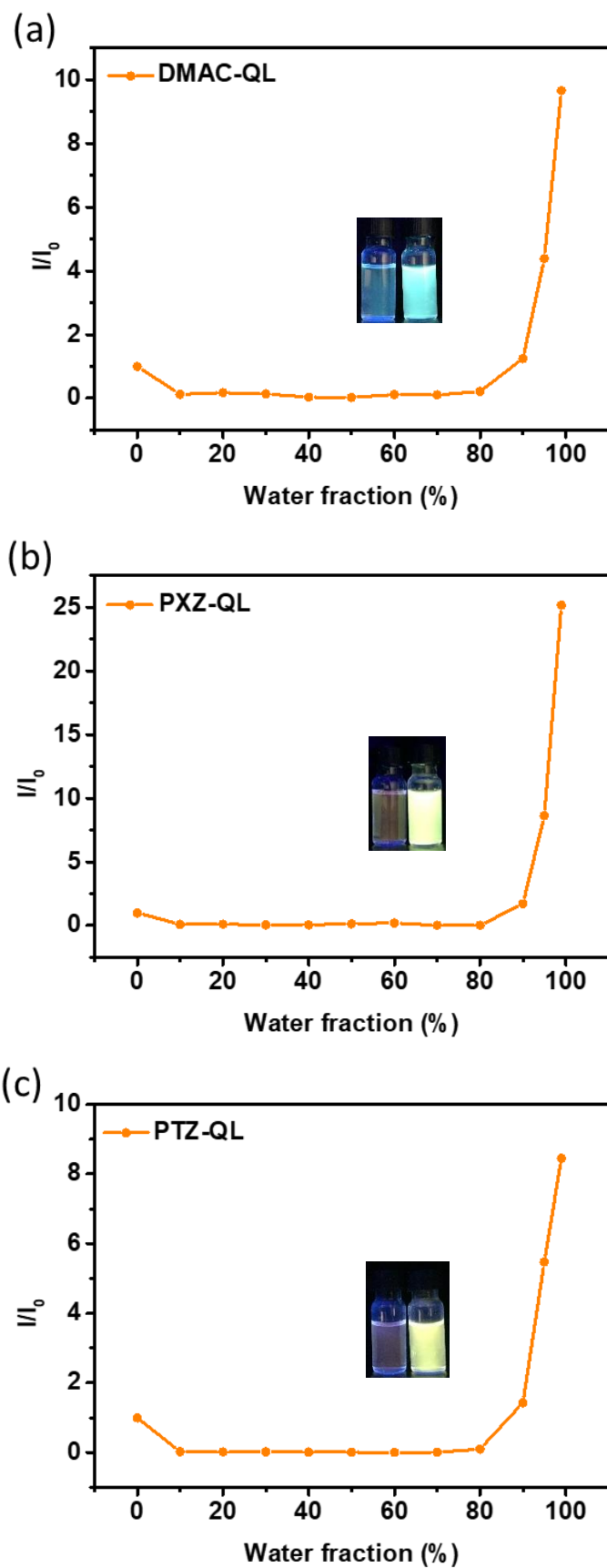


Fig. S4 PL intensity of (a) **DMAC-QL**, (b) **PXZ-QL** and (c) **PTZ-QL** in THF/H₂O solution with different water fractions (Inert: photos of emitters with water fraction of 0% and 99%).

4. NMR spectra

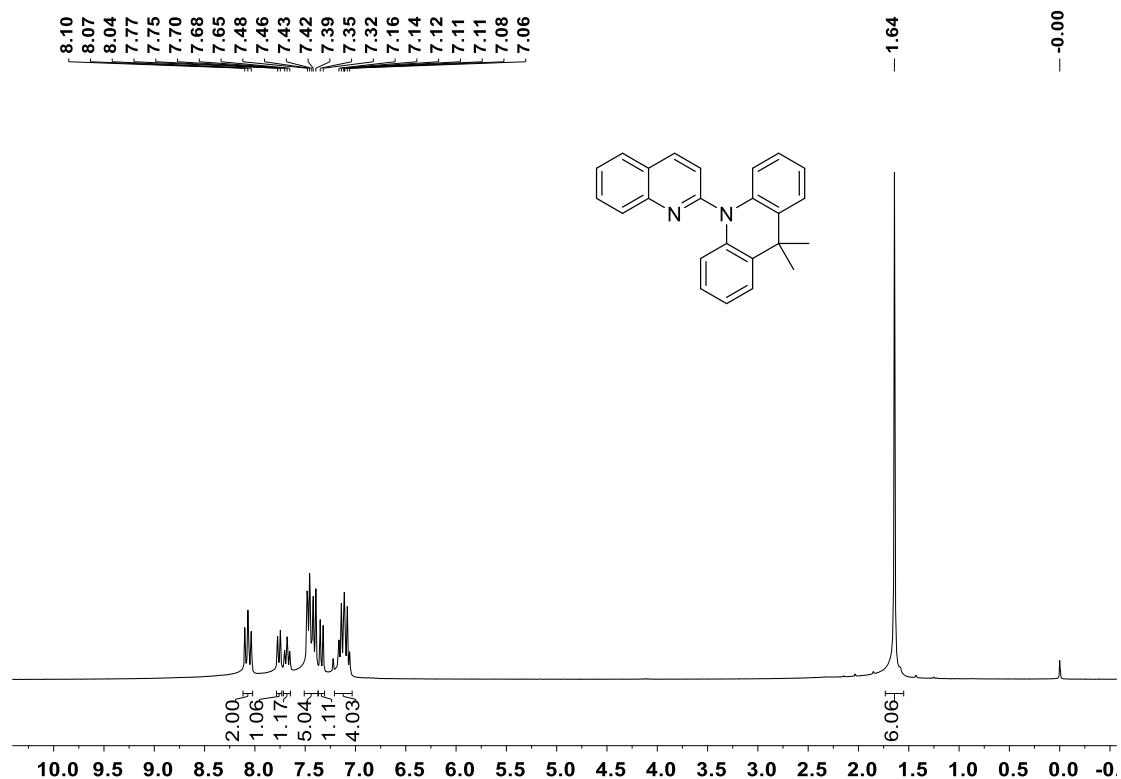


Fig. S5 ¹H NMR spectrum of DMAC-QL (300 MHz, CDCl₃).

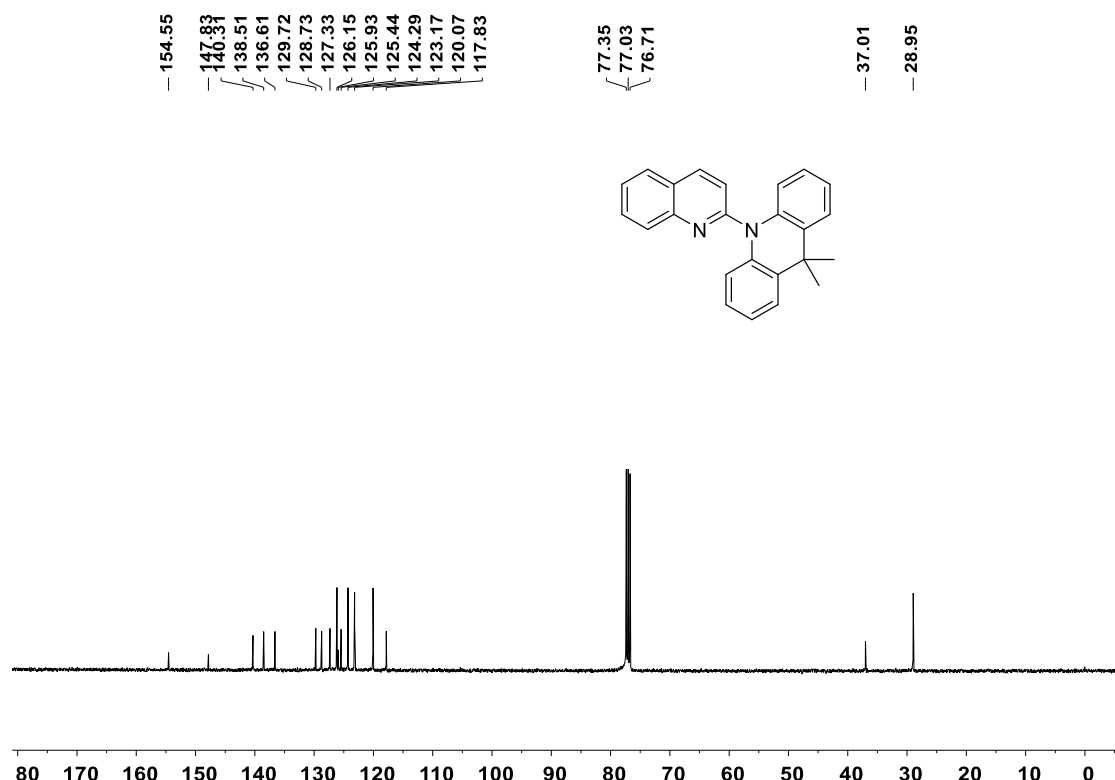


Fig. S6 ¹³C NMR spectrum of DMAC-QL (75 MHz, CDCl₃).

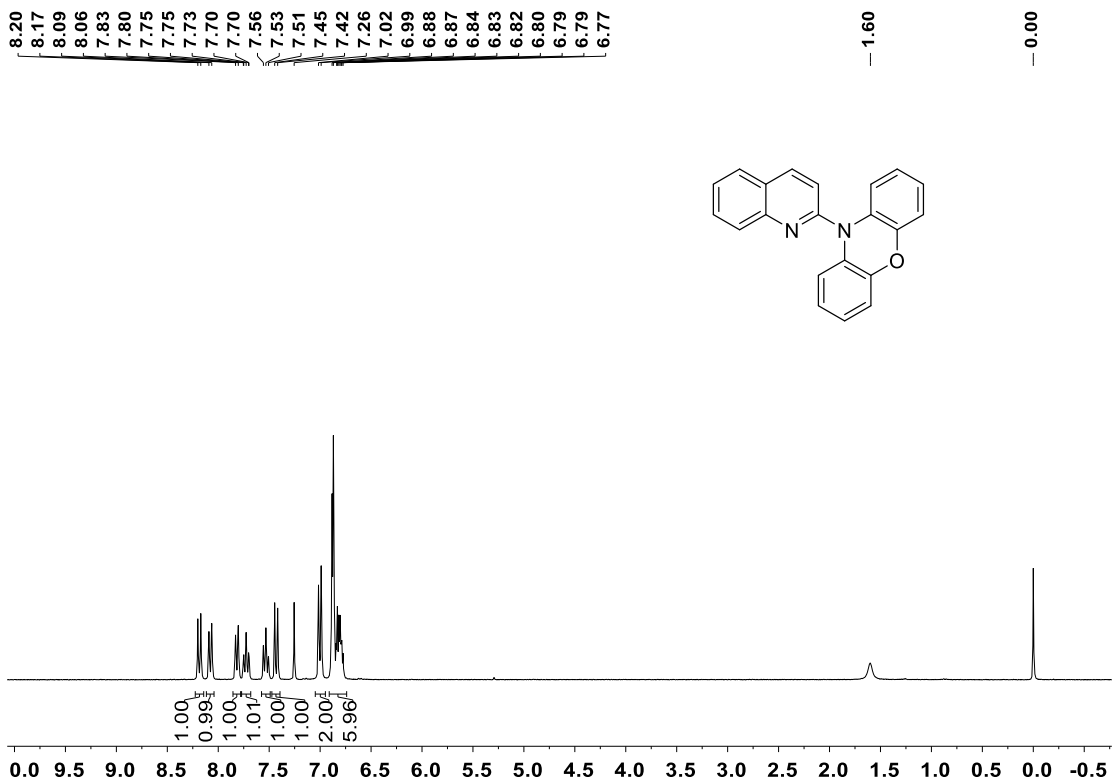


Fig. S7 ¹H NMR spectrum of PXZ-QL (300 MHz, CDCl₃).

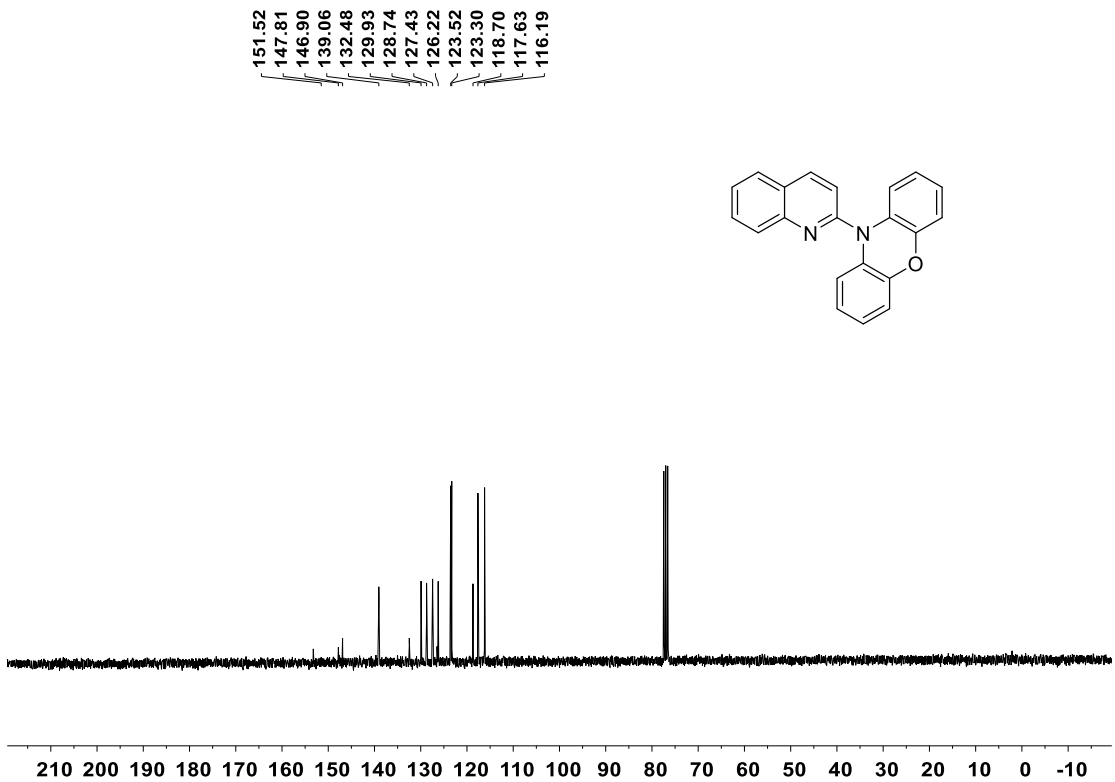


Fig. S8 ¹³C NMR spectrum of PXZ-QL (75 MHz, CDCl₃).



Fig. S9 ^1H NMR spectrum of PTZ-QL (300 MHz, CDCl_3).

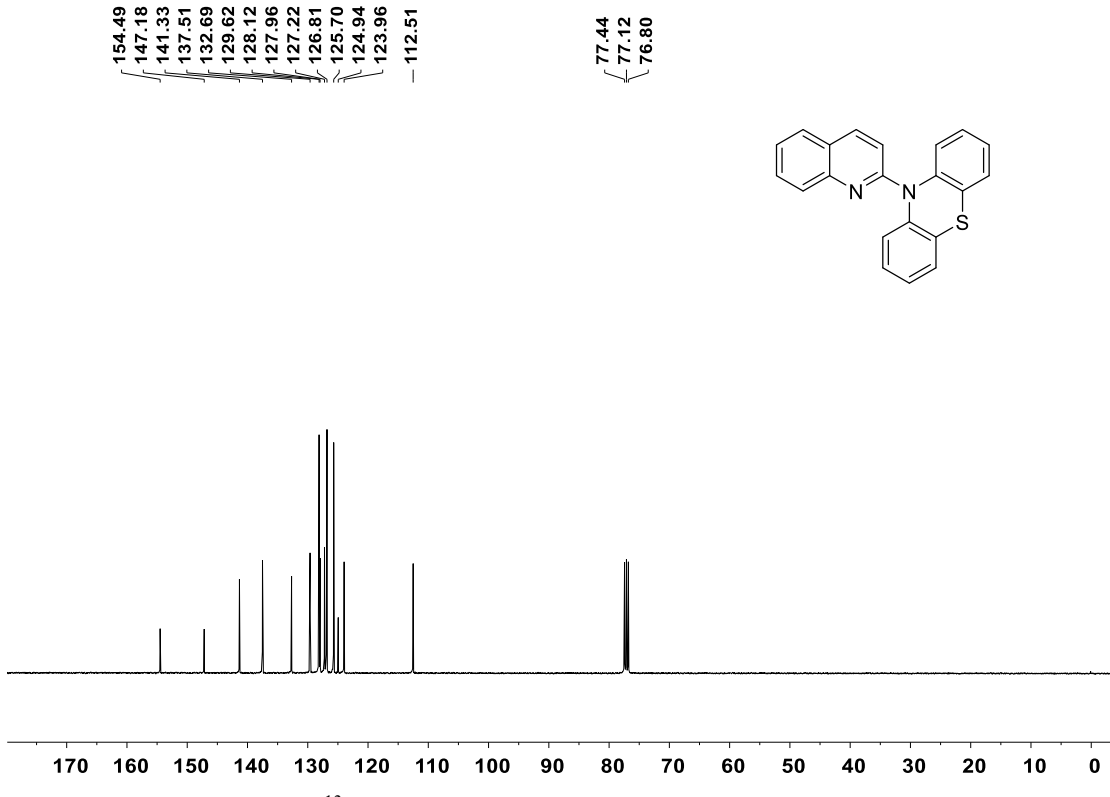


Fig. S10 ^{13}C NMR spectrum of PTZ-QL (75 MHz, CDCl_3).

5. High-resolution mass spectra



Fig. S11 High-resolution mass spectrum of **DMAC-QL**.

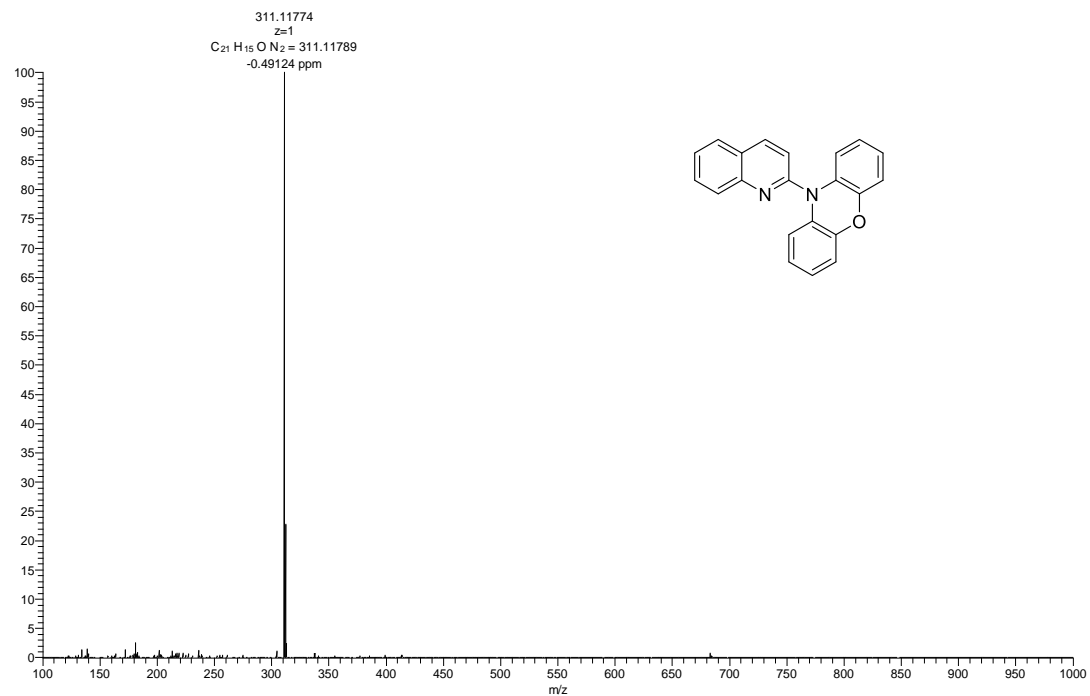


Fig. S12 High-resolution mass spectrum of **PXZ-QL**.

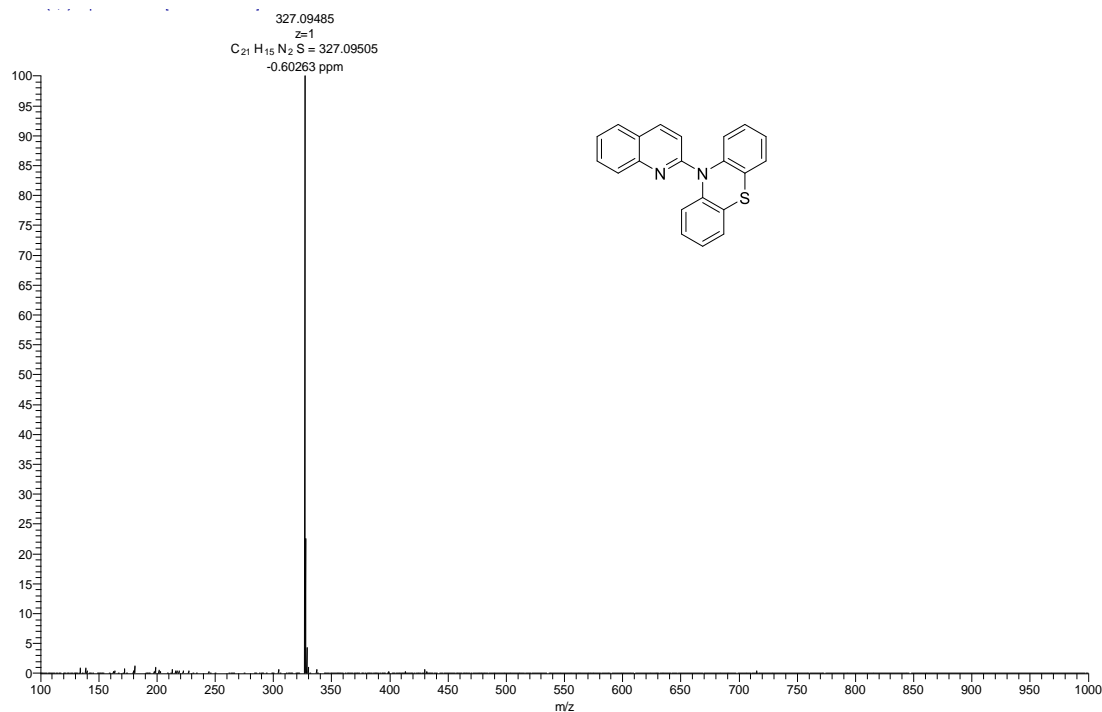


Fig. S13 High-resolution mass spectrum of **PTZ-QL**.

6. DFT calculations

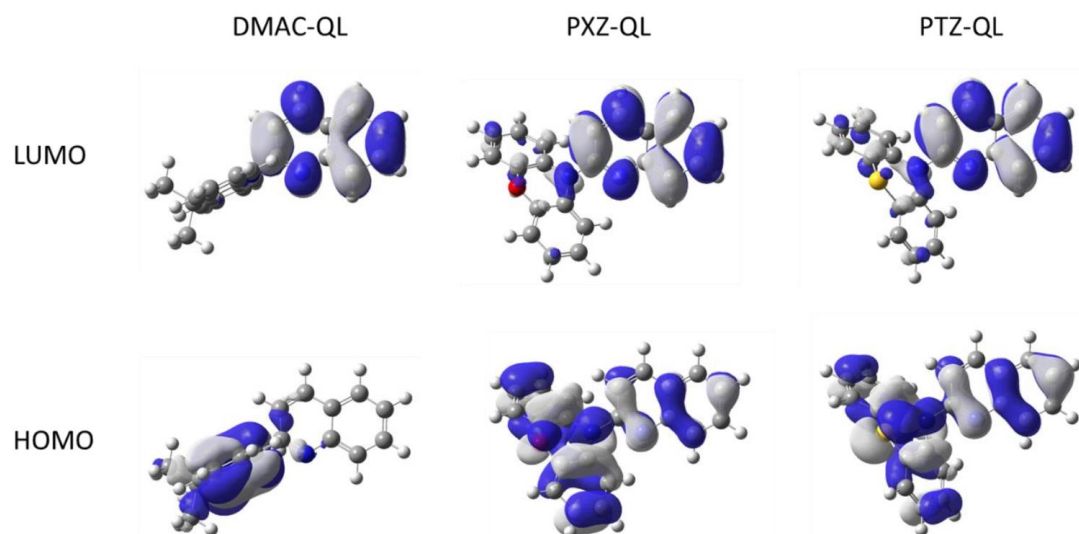


Fig. S14 DFT calculations of **DMAC-QL**, **PXZ-QL** and **PTZ-QL**.

7. HPLC analysis

Column: Chiralpak® IF, 10 mm × 250 mm

Mobile phase: hexane: dichloromethane = 10 : 90

Flow rate: 2.0 mL/min

Abs. detector: 365 nm

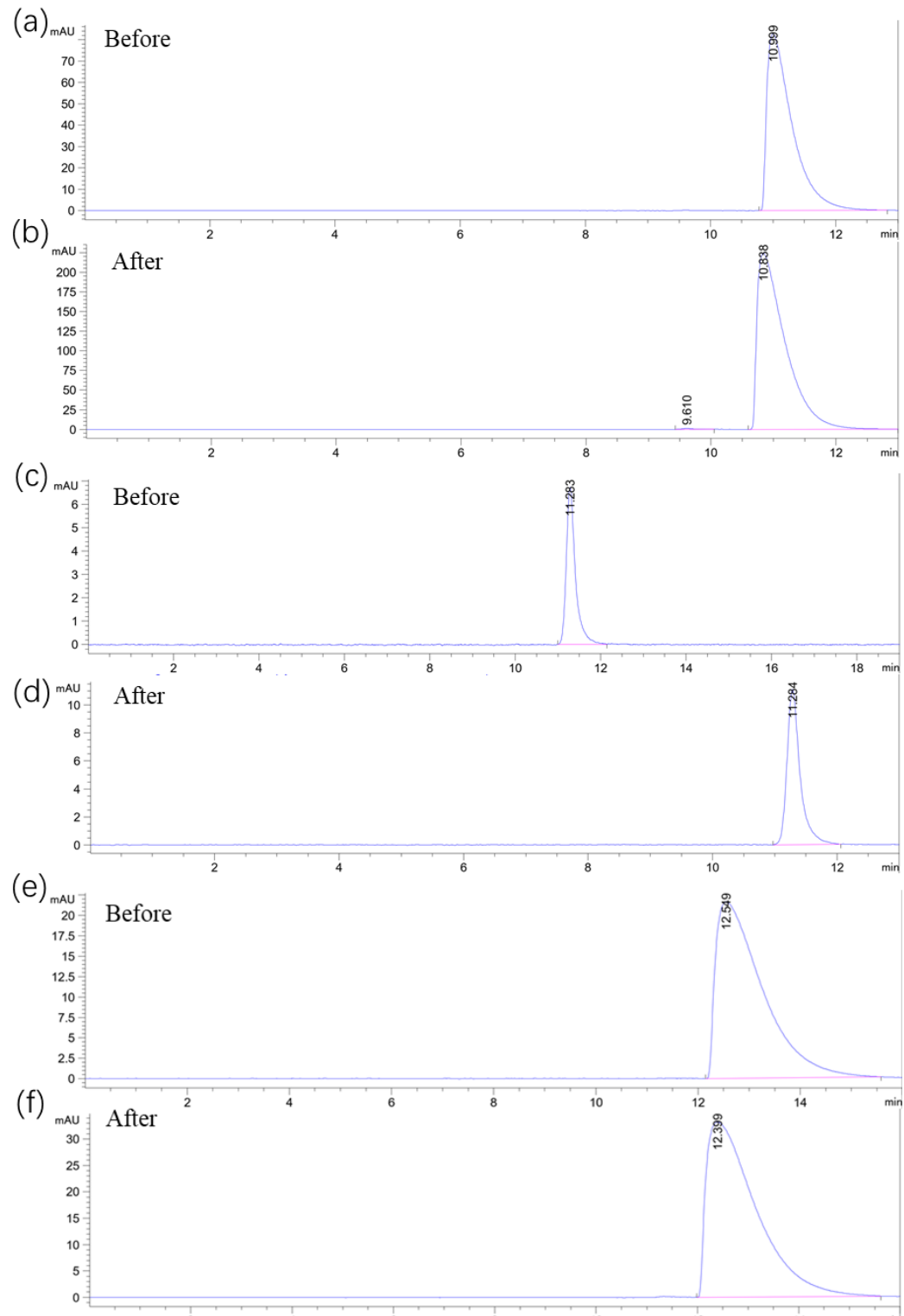


Fig.S15 High-performance liquid chromatography (HPLC) of **DMAC-QL** (a-b), **PXZ-QL** (c-d) and **PTZ-QL** (e-f) before and after the vacuum deposition process.

Table S3. The summary of HPLC profiles of **DMAC-QL**, **PXZ-QL** and **PTZ-QL** before and after the vacuum deposition process.

Sample	RetTime (min)	Width (min)	Area (mAU S)	Height (mAU)	Area (%)
DAMC-QL Before	10.999	0.4164	2329.33179	82.75607	100.0000
DAMC-QL After	10.838	0.4567	6968.60449	224.17609	99.9129
PXZ-QL Before	11.283	0.2199	100.24567	6.72594	100.0000
PXZ-QL After	11.284	0.2214	163.19466	11.11092	100.0000
PTZ-QL Before	12.549	0.8289	1382.70898	21.65556	100.0000
PTZ-QL After	12.399	0.8038	2268.37378	33.16997	100.0000

8. Device fabrication and characterization

The OLEDs had the structure: Glass/ITO/HATCN (10 nm)/TAPC (25 nm)/EML (25 nm)/DPEPO (5 nm)/ TmPyPB (55 nm)/LiF (0.8 nm)/Al (100 nm). In which, ITO is indium tin oxide, HATCN is dipyrrazino(2,3-f:2',3'-h)-quinoxaline-2,3,6,7,10,11-hexacarbonitrile and served as hole-injection layer, 1,1-bis[4-[N,N-di(p-tolyl)-amino]phenyl]cyclohexane (TAPC) was used as hole-transporting layer, DMAC-QL, PXZ-QL and PTZ-QL serve as the non-doped emitting layers (EML), bis[2-(diphenylphosphino)phenyl]ether oxide (DPEPO) performed as the hole-blocking layer (HBL), 1,3,5tri(m-pyrid-3-yl-phenyl)benzene (TmPyPB) serve as electron-transporting layer (ETL), Liq and Al acted as electron injection layer and the cathode, respectively. The energy diagram and chemical structures of the materials used in device were shown in Figure S13.

The OLED devices were fabricated by vacuum deposition onto pre-coated ITO glass substrates at a low pressure (1×10^{-5} mbar) for organic and metal deposition successively, with deposition rate of $0.5\sim3$ Å s⁻¹. Before the fabrication of devices, the ITO glass substrates were cleaned with Decon 90, rinsed in ultrapure water and ethanol, dried in an oven at 120 °C, then by plasma cleaning process.

The EL luminescence spectra and CIE color coordinates were recorded with a Spectrascan PR670 spectrophotometer, and the current-voltage-luminance (I-V-L) characteristics of the devices were measured with a computer-controlled Keithley 2400 SourceMeter under ambient atmosphere. Therefore, the current and power efficiencies of devices were obtained.

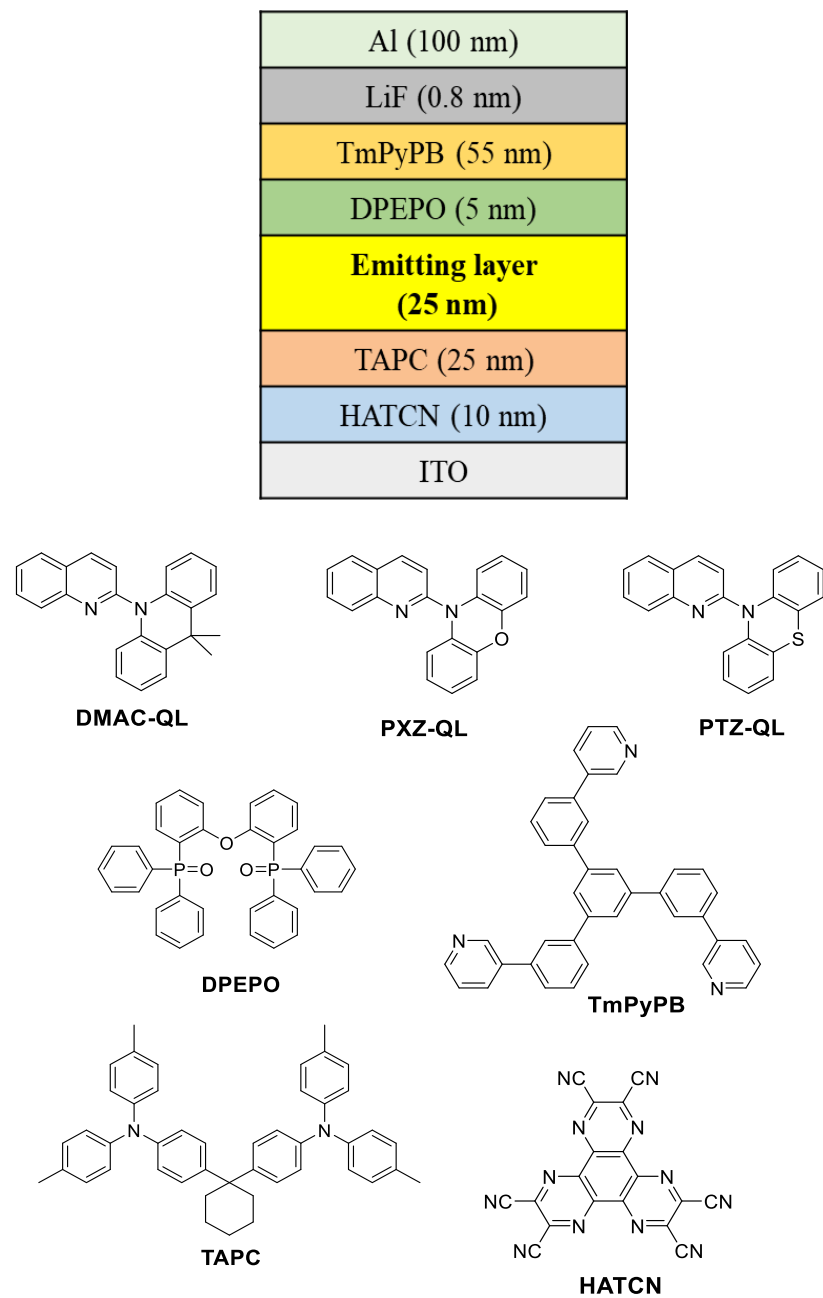


Fig. S15 Device structure and related molecular formula of materials.

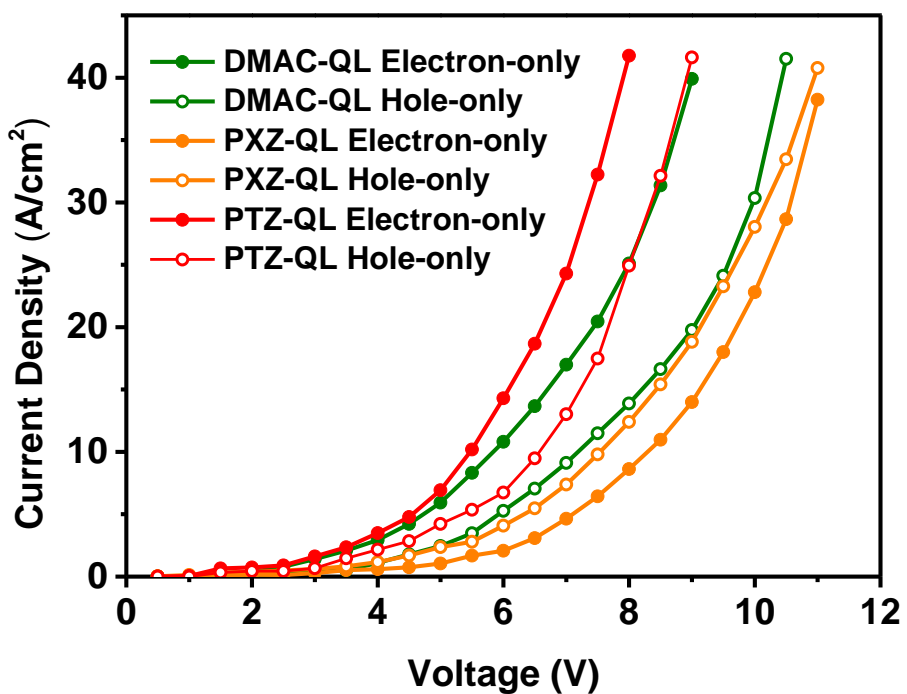


Fig. S16 J - V characteristics of **DMAC-QL**, **PXZ-QL** and **PTZ-QL** based mono layer single-carrier transporting devices with the structure of ITO/MoO₃ (6 nm)/Emitter (100 nm)/MoO₃ (6 nm)/Al (100 nm) for hole-only and ITO/LiF (1 nm)/Emitter (100 nm)/LiF (1 nm)/Al (100 nm) for electron-only, respectively.

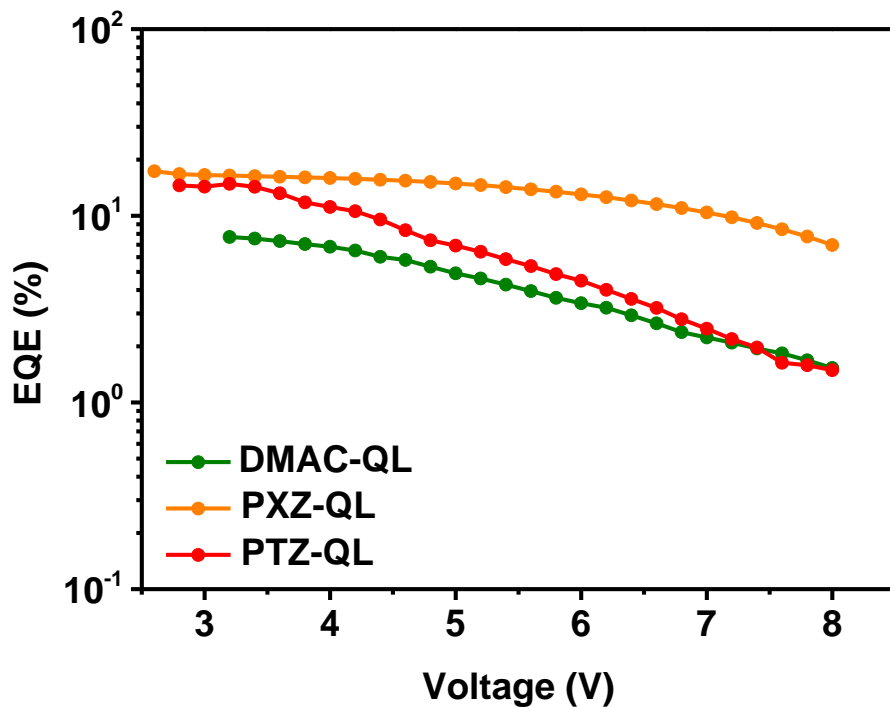


Fig. S18 Voltage-external quantum efficiency characteristics of the OLEDs based on **DMAC-QL**, **PXZ-QL** and **PTZ-QL**.

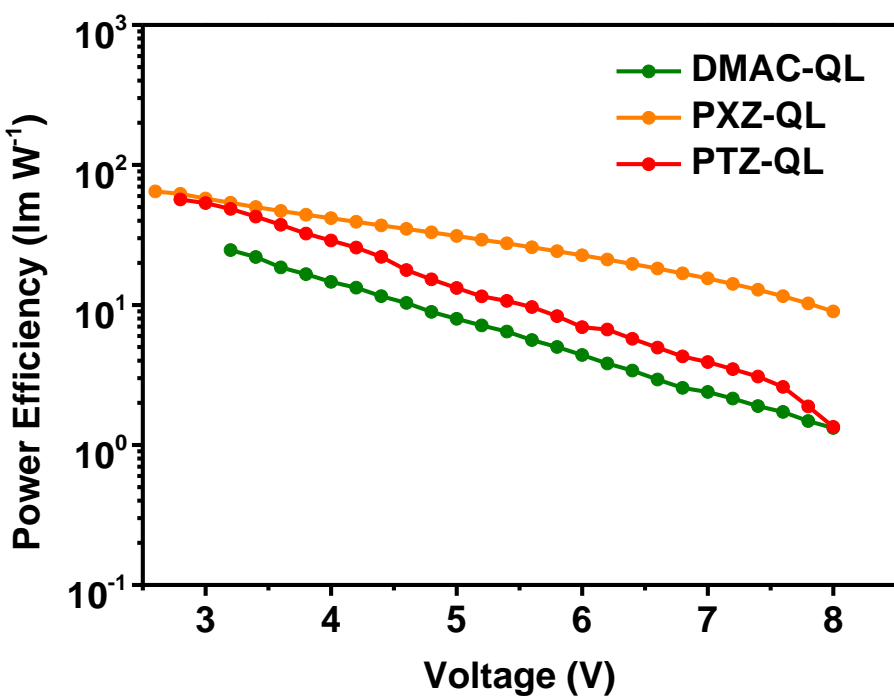


Fig. S19 Voltage-power efficiency characteristics of the OLEDs based on **DMAC-QL**, **PXZ-QL** and **PTZ-QL**.

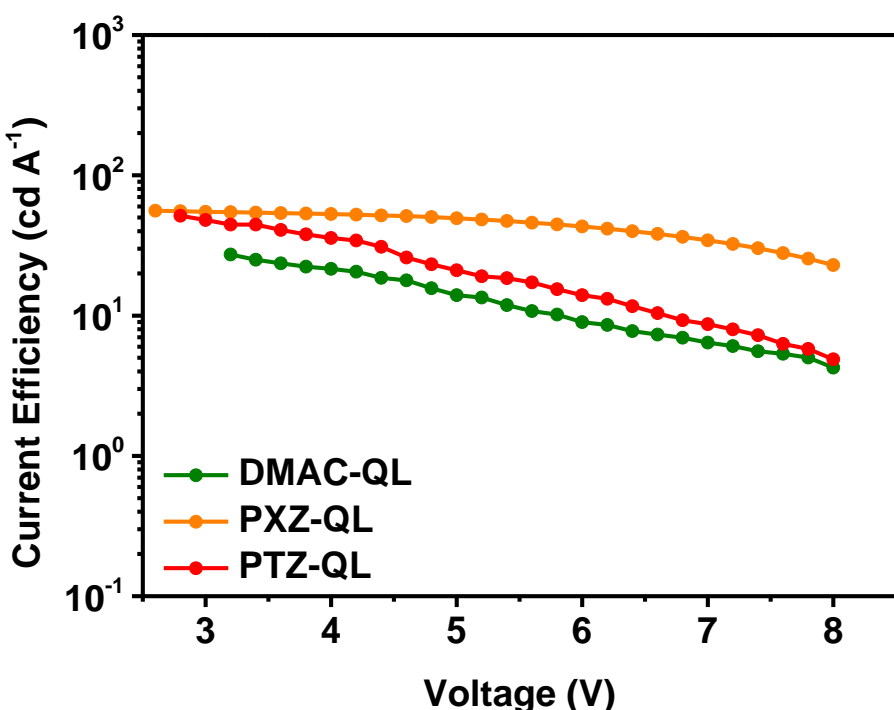


Fig. S20 Voltage-current efficiency characteristics of the OLEDs based on **DMAC-QL**, **PXZ-QL** and **PTZ-QL**.

Table S4 The comparison of our work and other reported AIDF emitters.

Emitter	V _{on} (V)	CIE(x, y)	λ _{EL} (nm)	PE _{max} (lm/W)	CE _{max} (cd/A)	EQE _{max} (%)
DMAC-QL	3.2	(0.31, 0.51)	522	24.6	27.2	7.7
PXZ-QL	2.6	(0.36, 0.55)	536	64.6	55.9	17.3
PTZ-QL	2.8	(0.39, 0.56)	546	56.7	51.5	14.8
CP-BP-PXZ ^[S1]	2.5	(0.40, 0.57)	-	65.7	59.1	18.4
CP-BP-PTZ ^[S1]	2.5	(0.42, 0.55)	-	55.7	46.1	15.3
CP-BP-DMAC ^[S1]	2.7	(0.23, 0.49)	-	37.9	41.6	15.0
PXZ2PTO ^[S2]	4.3	(0.27, 0.50)	504	32.0	44.9	16.4
SFDBQPXZ ^[S3]	3.4	-	584	22.5	24.3	10.1
DFDBQPXZ ^[S3]	3.2	-	588	20.6	21.0	9.8
DMAC-ND ^[S4]	2.9	(0.28, 0.53)	514	32.0	34.7	11.0
PTZ-ND ^[S4]	3.3	(0.36, 0.55)	534	26.2	30.7	9.7
PXZ-ND ^[S4]	3.0	(0.48, 0.48)	568	8.8	10.2	3.7
DMF-BP-PXZ ^[S5]	2.7	(0.440, 0.543)	~560	38.0	39.9	13.3
DPF-BP-PXZ ^[S5]	2.6	(0.458, 0.530)	~560	45.0	41.6	14.3
SBF-BP-PXZ ^[S5]	2.5	(0.456, 0.528)	~560	37.9	36.8	12.3
TRZ-HPB-PXZ ^[S6]	2.5	(0.39, 0.57)	544	44.9	41.2	12.7
TRZ-HPB- DMAC ^[S6]	3.1	(0.28, 0.58)	521	17.6	21.4	6.5
35DCPP-BP- PXZ ^[S7]	3.0	(0.39, 0.57)	538	49.7	57.6	17.3
26DCPP-BP- PXZ ^[S7]	3.0	(0.38, 0.57)	542	37.0	53.2	16.1
DCDMF-BP- PXZ ^[S8]	2.6	(0.39, 0.57)	540	63.7	62.2	19.0
DCDPF-BP-PXZ ^[S8]	2.5	(0.38, 0.57)	544	67.4	61.1	18.5
DCSBF-BP-PXZ ^[S8]	2.7	(0.40, 0.56)	548	8.6	10.8	3.3
pipd-BZ-PXZ ^[S9]	3.2	(0.42, 0.55)	570	17.35	19.86	7.04
pipd-BZ-PTZ ^[S9]	2.6	(0.51, 0.48)	576	18.64	17.35	6.90
pipd-BZ-DMAC ^[S9]	3.0	(0.39, 0.54)	528	6.25	7.16	2.58

Table S5 The comparison of our work and other reported non-doped emitters with similar emissions.

Emitter	Reported Properties	V _{on} (V)	λ _{EL} (nm)	EQE _{max} (%)	CE _{max} (cd/A)	PE _{max} (lm/W)	EQE ₁₀₀₀ (%)
DMAC-QL	AIE+TADF	3.2	522	7.7	27.2	24.6	3.2
PXZ-QL	AIE+TADF	2.6	536	17.3	55.9	64.6	15.2
PTZ-QL	AIE+TADF	2.8	546	14.8	51.5	56.7	5.3
DMAC-ND ^[S4]	AIE+TADF	2.9	514	11.0	34.7	32.0	10.6
PTZ-ND ^[S4]	AIE+TADF	3.3	534	9.7	30.7	26.2	8.0
PXZ-ND ^[S4]	AIE+TADF	3.0	568	3.7	10.2	8.8	3.5
DBT-BZ-PXZ ^[S11]	AIE+TADF	2.9	557	9.2	26.6	27.9	6.8
DBT-BZ-PTZ ^[S11]	AIE+TADF	2.7	563	9.7	26.5	29.1	8.5
DMAC-o-TRZ ^[S12]	TADF	3.0	504	14.7	39.3	37.0	11.3
DCPDAPM ^[S13]	AIE+TADF	3.2	522	8.15	26.88	15.63	6.488
TATC-BP ^[S14]	AIE+TADF+MCL	2.6	549	5.9	17.8	20.0	4.8
TATP-BP ^[S14]	AIE+TADF+MCL	2.8	541	6.0	18.9	19.2	5.8
PTZMes2B ^[S15]	TADF	2.8	540	19.66	62.88	-	17.31
DMAC-BPI ^[S16]	AIE+TADF	2.9	508	24.7	-	59.7	21.7
SBF-BP-DMAC ^[S17]	AIE+TADF	2.5	528	20.1	67.2	65.9	16.8
DCB-DPS-PXZ ^[S18]	AIE+TADF	2.5	520	13.9	40.5	48.2	11.0
mCP-DPS-PXZ ^[S18]	AIE+TADF	2.5	520	14.7	45.6	55.0	12.1
pPhDCzDPSPXZ ^[S1 8]	AIE+TADF	2.5	523	17.1	53.0	59.9	15.4
mPhDCzDPSPXZ ^[S1 8]	AIE+TADF	2.5	521	18.1	56.3	63.9	16.7

9. References

- [S1] J. Huang, H. Nie, J. Zeng, Z. Zhuang, S. Gan, Y. Cai, J. Guo, S.-J. Su, Z. Zhao and B. Z. Tang, Highly efficient nondoped OLEDs with negligible efficiency roll-off fabricated from aggregation-induced delayed fluorescence luminogens, *Angew. Chem., Int. Ed.*, 2017, **56**, 12971-12976.
- [S2] S. Xiang, Z. Huang, S. Sun, X. Lv, L. Fan, S. Ye, H. Chen, R. Guo and L. Wang, Highly efficient non-doped OLEDs using aggregation-induced delayed fluorescence materials based on 10-phenyl-10H-phenothiazine 5,5-dioxide derivatives, *J. Mater. Chem. C*, 2018, **6**, 11436-11443.
- [S3] L. Yu, Z. Wu, G. Xie, C. Zhong, Z. Zhu, D. Ma and C. Yang, An efficient exciton harvest route for high-performance OLEDs based on aggregation-induced delayed fluorescence, *Chem. Commun.*, 2018, **54**, 1379-1382.
- [S4] C. Chen, H.-Y. Lu, Y.-F. Wang, M. Li, Y.-F. Shen and C.-F. Chen, Naphthyridine-based thermally activated delayed fluorescence emitters for multi-color organic light-emitting diodes with low efficiency roll-off, *J. Mater. Chem. C*, 2019, **7**, 4673-4680.
- [S5] J. Guo, J. Fan, L. Lin, J. Zeng, H. Liu, C.-K. Wang, Z. Zhao and B. Z. Tang, Mechanical insights into aggregation-induced delayed fluorescence materials with anti-kasha behavior, *Adv. Sci.*, 2019, **6**, 1801629.
- [S6] P. Zhang, J. Zeng, J. Guo, S. Zhen, B. Xiao, Z. Wang, Z. Zhao and B. Z. Tang, New aggregation-induced delayed fluorescence luminogens with through-space charge transfer for efficient non-doped OLEDs, *Front. Chem.*, 2019, **7**, 199.
- [S7] Y. Fu, H. Liu, X. Zhu, J. Zeng, Z. Zhao and B. Z. Tang, Efficient aggregation-induced delayed fluorescent materials based on bipolar carrier transport materials for the fabrication of high-performance nondoped OLEDs with very small efficiency roll-off, *J. Mater. Chem. C*, 2020, **8**, 9549-9557.
- [S8] H. Liu, H. Liu, J. Fan, J. Guo, J. Zeng, F. Qiu, Z. Zhao and B. Z. Tang, An effective design strategy for robust aggregation-induced delayed fluorescence luminogens to improve efficiency stability of nondoped and doped OLEDs, *Adv. Opt. Mater.*, 2020, 2001027.
- [S9] Z. Yang, Y. Zhan, Z. Qiu, J. Zeng, J. Guo, S. Hu, Z. Zhao, X. Li, S. Ji, Y. Huo and S.-J. Su, Stimuli-responsive aggregation-induced delayed fluorescence emitters featuring the asymmetric D-A structure with a novel diarylketone acceptor toward efficient OLEDs with negligible efficiency roll-off, *ACS Appl. Mater. Interfaces*, 2020, **12**, 29528-29539.
- [S10] C. Li, J. Wei, X. Song, K. Ye, H. Zhang, J. Zhang and Y. Wang, Non-doped luminescent material based organic light-emitting devices displaying high brightness under very low driving voltage, *J. Mater. Chem. C*, 2016, **4**, 7013-7019.
- [S11] J. Guo, X.-L. Li, H. Nie, W. Luo, R. Hu, A. Qin, Z. Zhao, S.-J. Su and B. Z. Tang, Robust luminescent materials with prominent aggregation-induced emission and thermally activated delayed fluorescence for high-performance organic light-emitting diodes, *Chem. Mater.*, 2017, **29**, 3623-3631.
- [S12] Y.-Z. Shi, K .Wang, X. Li, G.-L. Dai, W. Liu, K. Ke, M. Zhang, S.-L. Tao, C.-J. Zheng, X.-M.

- Ou and X.-H. Zhang, Intermolecular charge-transfer transition emitter showing thermally activated delayed fluorescence for efficient non-doped OLEDs, *Angew. Chem., Int. Ed.*, 2018, **57**, 9480-9484.
- [S13] Y. Zhao, W. Wang, C. Gui, L. Fang, X. Zhang, S. Wang, S. Chen, H. Shi and B. Z. Tang, Thermally activated delayed fluorescence material with aggregation-induced emission properties for highly efficient organic light-emitting diodes, *J. Mater. Chem. C*, 2018, **7**, 2873-2881.
- [S14] Y. Chen, S. Wang, X. Wu, Y. Xu, H. Li, Y. Liu, H. Tong and L. Wang, Triazatruxene-based small molecules with thermally activated delayed fluorescence, aggregation-induced emission and mechanochromic luminescence properties for solution-processable nondoped OLEDs, *J. Mater. Chem. C*, 2018, **6**, 12503-12508.
- [S15] X. Tang, Y. Tao, H. Liu, F. Liu, X. He, Q. Peng, J. Li and P. Lu, Phenothiazinen-dimesitylarylborane-based thermally activated delayed fluorescence, High-performance non-doped OLEDs with reduced efficiency roll-off at high luminescence, *Front. Chem.*, 2019, **7**, 373.
- [S16] Z. Huang, Z. Bin, R. Su, F. Yang, J. Lan and J. You, Molecular design of non-doped OLEDs based on a twisted heptagonal acceptor: a delicate balance between rigidity and rotatability, *Angew. Chem., Int. Ed.*, 2020, **59**, 9992-9996.
- [S17] J. Zeng, J. Guo, H. Liu, Z. Zhao and B. Z. Tang, A multifunctional bipolar luminogen with delayed fluorescence for high-performance monochromatic and color-stable warm-white OLEDs, *Adv. Funct. Mater.*, 2020, **30**, 2000019.
- [S18] P. Leng, S. Sun, R. Guo, Q. Zhang, W. Liu, X. Lv, S. Ye and L. Wang, Modifying the AIE-TADF chromophore with host-substituents to achieve high efficiency and low roll-off non-doped OLEDs, *Org. Electron.*, 2020, **78**, 105602.